HHS Public Access

Author manuscript

Gastroenterology. Author manuscript; available in PMC 2022 March 01.

Published in final edited form as:

Gastroenterology. 2021 March ; 160(4): 1301–1314.e8. doi:10.1053/j.gastro.2020.11.034.

Fusobacterium nucleatum adheres to *Clostridioides difficile* via the RadD adhesin to enhance biofilm formation in intestinal mucus

Melinda A. Engevik[1,2], **Heather A. Danhof**[3], **Jennifer Auchtung**[3,4], **Bradley T. Endres**[5], **Wenly Ruan**[1,2], **Eugénie Bassères**[5], **Amy C. Engevik**[6], **Qinglong Wu**[1,2], **Maribeth Nicholson**[7], **Ruth Ann Luna**[1,2], **Kevin W. Garey**[5], **Sue E. Crawford**[3], **Mary K. Estes**[3,6], **Renate Lux**[8], **Mary Beth Yacyshyn**[9], **Bruce Yacyshyn**[9], **Tor Savidge**[1,2], **Robert A. Britton**[3], **James Versalovic**[1,2]

[1]Department of Pathology & Immunology, Baylor College of Medicine

[2]Texas Children's Microbiome Center, Department of Pathology, Texas Children's Hospital

[3]Department of Molecular Virology and Microbiology, Baylor College of Medicine

[4]Department of Food Science and Technology, University of Nebraska-Lincoln

[5]Department of Pharmacy Practice and Translational Research, University of Houston College of Pharmacy

[6]Department of Surgical Sciences, Vanderbilt University Medical Center

[7]Department of Pediatrics, Vanderbilt University Medical Center

[8]Department of Periodontics, University of California Los Angeles School of Dentistry

[9]Department of Medicine Division of Digestive Diseases University of Cincinnati College of Medicine

Abstract

Background: Although *Clostridioides difficile* infection (CDI) is known to involve the disruption of the gut microbiota, little is understood regarding how mucus-associated microbes interact with *C. difficile*. We hypothesized that select mucus-associated bacteria would promote *C. difficile* colonization and biofilm formation.

[*]**Corresponding author:** Melinda Engevik, Ph.D, Texas Children's Hospital, 1102 Bates Ave, Feigin Tower Room 839, Houston, TX 77030, Phone: 760-310-7641 ; melinda.engevik@bcm.edu.

Author Contributions Statement: MAE and JV conceived and designed research; MAE, HD, JA, BTE, WR, ACE and EB performed the experiments. MAE, HD, JA, BTE, WR, EB, ACE, QW, MN, RAL, KWG, SEC, MKE, RL, MBY, BY, TS, RB, and JV analyzed data and edited and revised manuscript. MAE prepared figures; JV approved final version of manuscript.

Conflict of Interest:

J. Versalovic serves on the scientific advisory boards of Biomica, Plexus Worldwide and Seed Health, and J. Versalovic and R. Britton receive unrestricted research support from Biogaia, AB. The remaining authors declare that the research was conducted in the absence of any commercial or financial relationships that could be construed as a potential conflict of interest.

Methods/Results: To create a model of the human intestinal mucus layer and gut microbiota, we used bioreactors inoculated with healthy human feces, treated with clindamycin and infected with *C. difficile* with the addition of human MUC2-coated coverslips. *C. difficile* was found to colonize and form biofilms on MUC2-coated coverslips and 16S rRNA sequencing revealed a unique biofilm profile with substantial co-colonization with *Fusobacterium*. Consistent with our bioreactor data, publicly available datasets and patient stool samples revealed that a subset of patients with *C. difficile* infection harbored high levels of *Fusobacterium*. We observed co-localization of *C. difficile* and *F. nucleatum* in an aggregation assay using adult patients and pediatric IBD patient stool and in CDI patient tissue sections. *C. difficile* strains were found to co-aggregate with *F. nucleatum* subspecies *in vitro;* an effect that was inhibited by blocking or mutating the adhesin RadD on *Fusobacterium* and removal of flagella on *C. difficile*. Aggregation was shown to be unique between *F. nucleatum* and *C. difficile*, as other gut commensals did not aggregate with *C. difficile*. Addition of *F. nucleatum* also enhanced *C. difficile* biofilm formation and extracellular polysaccharide production.

Conclusions: Collectively, these data demonstrate a unique interaction of between pathogenic *C. difficile* and *F. nucleatum* in the intestinal mucus layer.

Graphical Abstract

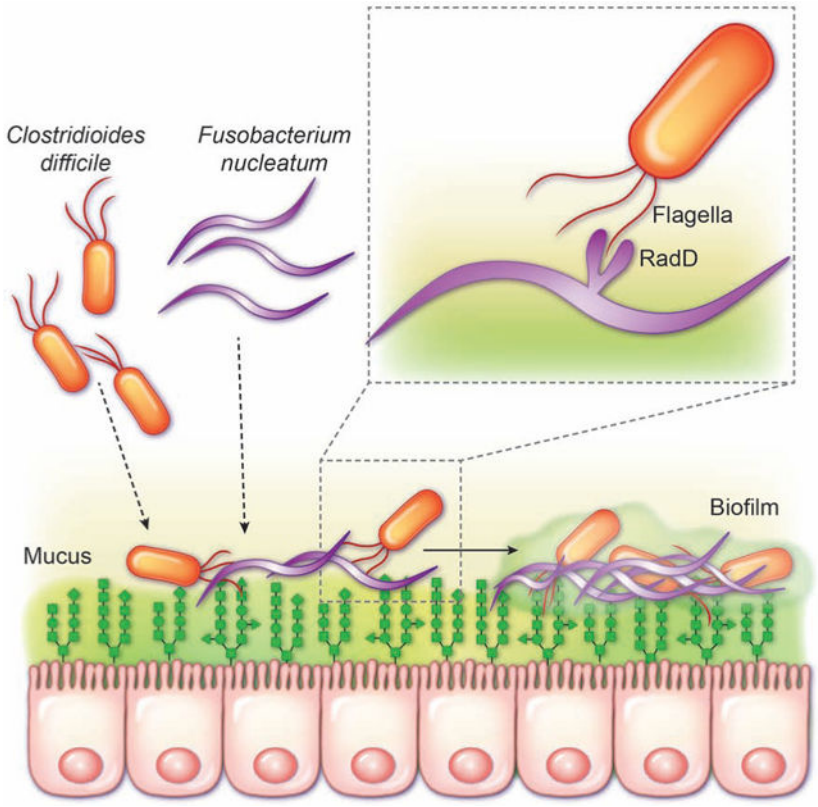

LAY SUMMARY

Our work shows that the pathogen *Clostridium difficile* chemotaxes, aggregates and forms resilient biofilms with another pathogen *Fusobacterium nucleatum* in the intestinal mucus layer.

Keywords

Clostridium difficile; MUC2; mucus; biofilm

Introduction

Clostridioides difficile is the most common healthcare associated pathogen in U.S. hospitals, incurring billions of dollars in treatment costs each year[1]. Antibiotic disruption of the gut microbiota creates a favorable niche for *C. difficile* spore germination, proliferation, and ultimately toxin production and disease[2]. While several studies have investigated germination and toxin production, the colonization phase of *C. difficile* infection (CDI), which likely involves interaction with other gut microbes, remains relatively unknown. Comparisons of CDI and non-CDI stool have revealed alterations of the gut microbiota[3, 4]. CDI patients are frequently co-infected with other pathobionts, including *Escherichia/Shigella, Salmonella, Staphylococcus, Klebsiella*, and *Fusobacterium*[3, 4]. These findings imply that gut microbiome composition may influence *C. difficile* pathogenesis.

C. difficile localizes to the outer colonic MUC2 mucus layer with members of *Bacteroidaceae* and *Enterobacteriaceae* in murine models[5]. *C. difficile* is also present in the mucus layer of CDI patients[6]. However, the mechanism by which *C. difficile* associates with human MUC2 is uncharacterized. Moreover, little data exists regarding which members of the human gut microbiota interact with *C. difficile*. Despite the potential to influence the course of infection, the interactions between *C. difficile* and other mucus-associated bacteria remain poorly defined. To address these gaps in knowledge, we have focused on an entirely human-centered approach, employing human-derived MUC2, fecal bioreactors and patient samples. Our work points to the potential for mucus-associated microbes to interact with and modulate *C. difficile*.

Methods:

Bacterial Strain, Media, and Culture Conditions

Bacteria were grown in an Anaerobe Systems AS-580 chamber at 37°C in 10% CO_2, 10% H_2, and 80% N_2 (supplemental methods). Bacteria were fluorescently-tagged with 10 μM CFDA-SE (Ex:Em: 428/528) or CMRA (Ex:Em: 548/576) (ThermoFisher) in PBS anaerobically at 37°C for 1 hr as described[7]. For growth curves, cultures of *C. difficile* R20291 and *F. nucleatum* subspecies *nucleatum* in BHIS were used to inoculate a chemically defined minimal medium (CDMM)[8] at Optical density $(OD)_{600nm}$ =0.1. Growth was assessed by OD_{600nm} and colony forming units (CFUs). For RNAseq, *C. difficile* R20291 was grown in CDMM supplemented with spent *C. dificile* R20291 CDMM medium (after 16 hrs incubation) or spent *F. nucleatum* subspecies *polymorphum* CDMM medium (supplemental methods).

Chemotaxis Assay:

For chemotaxis assays, *C. difficile* strains were grown in BHIS for 8 hrs, fluorescently-tagged with 10 μM CMRA, and suspended at OD_{600nm} =2.0 in chemotaxis buffer (10 M

potassium phosphate, 0.1 mM EDTA at pH 7.0) as previously described[9]. *C. difficile* was allocated to 96-well plates (200 μL) and capillary tubes filled with chemotaxis buffer with or without untagged *F. nucleatum* species (at OD_{600nm}= 2.0) or 15 mM ethanolamine were added and incubated anaerobically at 37°C for 1 hr. Following incubation, capillary tube contents were assessed by a fluorescence plate reader and confirmed by microscopy (Nikon Eclipse 90i). To calculate the population of *C. difficile* that chemotaxed, the fluorescence from the capillary tubes (chemotaxed) was compared to the starting solution fluorescence (total) using the calculation chemotaxed/total x 100%.

Aggregation Assay:

Aggregation assays were performed as previously described for *F. nucleatum*[10]. Briefly, bacteria were washed with PBS and resuspended in anaerobic aggregation buffer (150 mM NaCl, 1 mM Tris/HCl, 0.1 mM CaCl2, and 0.1 mM MgCl2, pH 7) at OD_{600nm} =1.5. Equal volumes (0.5 mL) of each bacteria were added to cuvettes, vortex-mixed for 10 sec, and read at OD_{600nm} (time 0 hr). Samples were incubated for 1 hr at 37°C anaerobically and OD_{600nm} was recorded (time 1 hr). Aggregation was calculated using the following equation: 100%-((OD_{600nm} at 0 hr –OD_{600nn} at 1 hr) x 100%). For inhibition assays, *F. nucleatum* cells were pre-incubated with 50 mM L-arginine, D-galactose, or D-glucose for 5 min at 37°C, followed by addition of other bacterial strains. To assess aggregation of *C. difficile* and *F. nucleatum* within stool samples, we selected 8 stool samples from adult CDI patients and 4 stool samples from pediatric CDI patients with IBD (supplemental methods). The selected samples harbored high *F. nucleatum* levels by qPCR. Ten mg of each stool sample was suspended in 1.5 mL aggregation buffer and mixed thoroughly. To remove stool particulate, samples were centrifuged at 300 x g for 5 min. The supernatant was removed, 1 mL was transferred to microfuge tubes and incubated at 37°C for 1 hr. Following incubation, supernatants were removed and aggregates were transferred to microscope slides for FISH staining.

Mammalian Cell Culture

Mucus-producing human colon cells HT29-MTX (#12040401 Sigma), T84 (ATCC CCL-248), and LS174T (ATCC CL-188) were maintained in DMEM medium supplemented with 10% heat-inactivated fetal bovine serum (Invitrogen) at 37°C, 5% CO_2. For adhesion assays, 5 x 10^5 cells were seeded onto Corning Costar 12-well plates containing poly-lysine-coated coverslips and grown to confluence. MUC2 was purified from HT29-MTX and LS174T cells and human stool specimens as previously described[7]. Glycans were removed from MUC2 with 10 mM HCl heated in a boiling water bath (100°C) for 30 min and neutralized with 100 mM NaOH. MUC2 was ethanol-precipitated and treated with 100 mM NaOH for 20 hr at 23°C. The solution was neutralized with HCl and the denuded protein was ethanol-precipitated. Supernatants containing O-linked glycans were lyophilized and glycan concentrations were determined using the phenol sulfuric acid method.

MUC2-coated coverslips and 96-well plates

Glass coverslips (18 mm) were coated with 1 mg/mL MUC2 using 3-aminopropyltriethoxysilane (APTS) as previously described[11]. High-binding 96-well plates (Costar) were also coated in 1 mg/mL mucin or O-linked glycans in Hank's Salt Solution by

overnight incubation at 4°C. For MUC2 adhesion, fluorescently-tagged bacteria at OD_{600nm} =2 were incubated with coverslips or plates anaerobically at 37°C for 1 hr. After washing, adhesion was examined by plate reader and microscopy

Human Colonoid Monolayers

The colonoid (C104) line was obtained from Texas Medical Center Digestive Diseases Center Gastrointestinal Experimental Model Systems Core. All procedures used to generate organoid cultures were approved by the Baylor College of Medicine IRB committee. Differentiated human colonoid monolayers were generated as previously described[12]. Monolayers (passage 12) were stained with Hoechst for 10 min at room temperature and incubated for 1 hour with fluorescently-tagged *C. difficile* R20291 and/or *F. nucleatum* subspecies at 37°C, 5% CO_2. Monolayers were thoroughly washed and fixed with 4% paraformaldehyde for 30 min at room temperature. Adhesion was examined by microscopy.

Biofilm Assays

Overnight cultures of *C. difficile* and *F. nucleatum* were diluted in BHIS to OD_{600nm} =0.1 and 100 μL of each culture was added to the 96-well plates coated with 1 mg/mL MUC2. For *C. difficile* control wells, 200 μL of culture was added. Plates were sealed and anaerobically incubated at 37°C for 72 hours. Biofilms were washed with PBS, stained with 0.1% crystal violet and assessed by OD_{600nm} on a plate reader. Biofilms were also stained with Ruby Red Biofilm Tracer (ThermoFisher) and imaged by microscopy. Biofilm were quantified with FIJI software (National Institutes of Health) by tabulating the mean pixel intensity. Polysaccharides were isolated from biofilms as described[13] and examined by the phenol-sulfuric acid method. Proteins were extracted from biofilms using RIPA buffer complemented with Complete Protease Inhibitor Cocktail (Roche) and quantified by the BCA assay using bovine serum albumin standards (ThermoFisher cat#23209). Biofilms were also grown for 48 hrs anaerobically at 37°C, then treated with proteinase K (30 mA/mL), DNAse (50 kU/mL), EDTA (12.5 mM), and vancomycin (400 μg/mL) for an additional 24 hrs anaerobically at 37°C.

C. difficile growth on mucin-coated surfaces in human fecal bioreactors

Bioreactors were constructed from 100 mL media bottles fitted with 2-port Q-series GL45 bottle caps (Kinesis) using fecal samples, media and conditions previously optimized[14] (supplemental methods). Bioreactors were inoculated with fecal samples, treated with clindamycin (250 μg/mL) to disrupt the community, and then HT29-MTX MUC2-coated or mock-PBS-coated coverslips were introduced into reactors. At the time of coverslip introduction, communities were also treated with 3 x 10^6 CFUs of *C. difficile* 2015 pre-grown in bioreactor medium[14]. After 3 days of co-incubation, MUC2-coated coverslips were removed for analysis.

Evaluation of bacterial RNA and gDNA

Bacterial RNA was isolated as previously described[7]. RNA sequencing was performed at the University of Houston Seq-N-Edit Core. Triplicates were pooled for each condition to limit the sample size. The NuGEN ovation complete prokaryotic RNAseq library preparation kit

(Tecan Genomics) was used according to manufacturer's recommendations. Library quality and quantification were assessed via a 2100 BioAnalyzer instrument (Agilent). cDNA libraries were sequenced on a NextSeq 500 system (Illumina) for 150 cycles according to manufacturer's protocol. Analysis of the data was performed using PATRIC bacterial bioinformatics resource center[15]. FastQ files were used as input for the program Rockhopper to align, assemble, quantify reads and generate differential expression patterns.

gDNA from biofilms and stool was extracted using the Zymo gDNA isolation kit (Zymo) according to the manufacturer's instructions with the addition of 2 rounds of bead homogenization. To assess *Fusobacterium* levels in patient stool samples, gDNA was examined by qPCR using FAST SYBR green master mix with primers (*Fusobacterium* forward: CAACCATTACTTTAACTCTACCATGTTCA; Reverse: GTTGACTTTACAGAAGGAGATTATGTAAAAATC) on a QuantStudio3 qPCR machine (Applied Biosystems). 16S rDNA amplicons from bioreactor biofilms were sequenced by MiSeq paired-end sequencing (supplemental methods). Additionally, 16S rDNA data (454 and Illumina; 16S regions of V3-V5 and V4) from published studies were downloaded from NCBI Sequence Read Archive database and sorted for relative *Fusobacterium* levels.

Patient information and human specimen collection

All patient specimens were collected under the appropriate IRBs at the University of Cincinnati Medical Center Hospital, Cincinnati, OH (Human Research Protection Program #2012-4147) and Vanderbilt University Medical Center, Nashville TN (Human Research Protections Program #170067) (supplemental methods).

Immunostaining, FISH and SEM

Cell monolayers were stained with Hoechst, incubated with fluorescently-tagged bacteria for 1 hr at 37°C, fixed with 4% paraformaldehyde and stained with rabbit anti-MUC2 antibody (Novus cat#NBP1-31231). FISH staining was performed on stool aggregates, bioreactor MUC2-coverslips, and patient slides. Slides were hybridized with the probe [6FAM]CATCCTGTACTGGCTCAC for *C. difficile*[5], [Cy3]CTTGTAGTTCCGCCTACCTC for *F. nucleatum*[16] or [Cy3]GCTGCCTCCCGTAGGAGT for total bacteria[16] (Integrated DNA Technologies). For SEM, 10^4 *C. difficile* cells were incubated with LS174T monolayers or HT29-MTX-derived MUC2-coated coverslips for 1 hr at 37°C. For biofilms, cultures were incubated with HT29-MTX MUC2-coated coverslips or 96-well plates anaerobically for 72 hrs at 37°C. Following incubation, samples were washed with PBS, fixed in 2.5% glutaraldehyde, dehydrated in ethanol and coated with 20 nm of gold in a desktop sputtering system (Denton Desk II). Images were acquired on a scanning electron microscope (FEI XL-30FEG) at 12 kV.

Statistics

Comparisons between groups were made with either One-way or Two-way Analysis of Variance (ANOVA) with the Holm-Sidak *post-hoc* test via SigmaPlot (Systat Software, Inc., San Jose, CA). Graphs were generated using Graphpad (GraphPad Software, Inc. La Jolla, CA).

Results:

C. difficile adheres to human intestinal MUC2 glycans

Adherence to mucus promotes colonization for numerous gastrointestinal pathogens. *C. difficile* has been identified in the colonic MUC2 mucus layer in a murine model of CDI[5]. However, little information exists on *C. difficile* adhesion to human MUC2. To examine the adhesive properties of *C. difficile*, human MUC2 was purified from several sources, including human mucin-producing LS174T, HT29-MTX and T84 cells and from human stool samples. Purified MUC2 was coated on glass coverslips and adhesion of fluorescently-tagged *C. difficile* to MUC2-coated coverslips was examined by microscopy after 1 hour incubation. We observed that *C. difficile* R20291 adhered to MUC2 isolated from all sources and was largely absent in control PBS-coated coverslips (Fig. 1A). To increase the resolution of the observed interaction between *C. difficile* and MUC2, we performed scanning electron microscopy (SEM) on HT29-MTX-MUC2 coverslips and observed *C. difficile* in the MUC2 layer (Fig. 1B). To examine if mucus binding is broadly conserved across multiple *C. difficile* lab strains and ribotypes (Fig. 1C, Supplemental Table 1), we examined adhesion of fluorescently-tagged *C. difficile* to MUC2 coated 96-well plates and found that all *C. difficile* strains could adhere to MUC2. We observed the greatest adhesion with *C. difficile* 630, M68, MT1850 and MT1950. These data indicate that MUC2 adhesion is functionally conserved across ribotypes. No adhesion was observed to methylcellulose, a polysaccharide commonly used to mimic the viscosity of a mucus environment (***data not shown***).

Mucin proteins are decorated with a wide range of glycans that serve as potential sites for adhesion by intestinal microbes. To identify *C. difficile* binding sites in human MUC2, O-linked glycans were removed by β-elimination and purified. We then repeated the adhesion assays with isolated O-linked glycans. Robust adhesion of *C. difficile* to extracted O-glycans was observed, and this pattern was similar to adhesion levels in the complete MUC2 protein (Fig. 1D). The data indicate that *C. difficile* adheres to the glycan component of the MUC2 mucin protein. We also sought to examine the interactions of *C. difficile* and MUC2 in live cells. Consistent with adhesion to purified MUC2, we observed that *C. difficile* R20291 co-localized with MUC2 in human mucin-producing LS174T cells by SEM after 1 hr incubation (Fig. 1E). Next, we examined *C. difficile* adhesion to MUC2 in a more physiologically relevant intestinal primary cell culture system. Colonoids derived from intestinal stem cells represent non-transformed epithelial cultures that harbor all the native intestinal cell types including MUC2 secreting goblet cells[17]. Similar to the observed patterns of adhesion in mucin-producing cell lines, *C. difficile* co-localized with MUC2 positive goblet cells in human colonoids (Fig. 1F, G); this can be seen more clearly in the expanded insert (Fig. 1F). These data are the first to demonstrate that *C. difficile* adheres to human MUC2, specifically binding to the O-linked glycans.

Microbes found in the mucus layer, including *C. difficile*, can be visualized growing as micro-colonies or biofilms. To identify bacterial members encountering *C. difficile* in a mucus-based microbial community, we turned to a modified bioreactor system. Fecal samples were cultivated and treated with clindamycin (250 μg/mL) to perturb microbial communities and mirror antibiotic-mediated microbial depletion during patient infection.

Then, MUC2-coated coverslips were introduced into reactors and 3 x 10^6 CFU of *C. difficile* was added and incubated for 3 days to allow for mucus-associated microbial communities to form. FISH probes identified *C. difficile* and other microbial members marked by 16S FISH staining in the mucin-coated coverslips (Fig. 2A). Robust biofilms were observed, as denoted by ruby red biofilm tracer and crystal violet staining (Fig. 2A). By 16S rRNA gene sequencing, the dominant phyla of the mucus-associated microbiome included the phyla Firmicutes (26.3%), Bacteroidetes (36.7%), Proteobacteria (16.6%) and Verrucomicrobia (2.0%) (Fig. 2B). At the family level, within Firmicutes we observed high abundance *Lachnospiraceae* (8.3%), *Ruminococcaceae* (1.5%), *Clostridiaceae* (1.5%), and *Clostridium XII sensu stricto* (1.1%). *Peptostreptococcaceae* which contains *C. difficile*, compromised 4% of the sequences (Fig. 2C). In the Bacteroidetes, we observed primarily *Bacteroidaceae* (33.3%) and *Tannerellaceae* (3.4%). The majority of Proteobacteria were from the family *Enterobacteriaceae* (15.7%). Consistent with the presence of MUC2, we did observe the mucin degrader *Akkermansia* (1.9%). Surprisingly, 17.7% of sequences arose from the phylum Fusobacteria, family *Fusobacteriaceae*, a common oral microbiome constituent.

Fusobacterium plays a key role in multi-species biofilm formation in the oral cavity[18], so we reasoned that members of the genus *Fusobacterium* may be an active participant in mucin-based intestinal biofilms with *C. difficile*. Three subspecies of *F. nucleatum* (*nucleatum, polymorphum* and *animalis*) were able to adhere to purified MUC2 and to the MUC2-producing cell line HT29-MTX (Supplemental Fig. 1A-C), suggesting that *F. nucleatum* can reside in the intestinal mucus layer. A previous report has pointed to the co-occurrence of *F. nucleatum* and *C. difficile* in colorectal cancer patients[19]. To determine whether *F. nucleatum* was present in non-cancer patients with CDI, we examined 16S sequencing data from publicly available datasets[3, 4, 20-22]. Data analysis from three published studies from Battaglioli[21], Schubert[4] and Schneider[23] *et al*. revealed that patients with non-descriptive CDI harbored higher relative abundance of compared to the control population (Fig. 3A,B). Two additional studies from Khanna[24] and Seekatz[22] which only examined CDI patients revealed similar relative abundance levels of *Fusobacterium* OTUs for primary CDI[24] and recurrent CDI[22, 24] (Fig. 3A,B). In all studies, only subsets of patients had detectable *Fusobacterium* OTUs (Battaglioli[21]: Control=13.8%, CDI=31.1%; Schubert[4].: Control=7.1%, CDI=35.5%, Schneider[3]: Control=7.4%; CDI=25.9%; Khanna[24]: pCDI=36.4%; Seekatz[22]: pCDI=33.9%; rCDI=38.9%)(Fig. 3C). Examination of another independent adult cohort of CDI patients from the University of Cincinnati revealed similar percentages of *Fusobacterium* positive samples by qPCR (38.4%)(Fig. 3C). Interestingly, we observed higher abundances of *Fusobacterium* in patients who experienced diarrhea, but were negative for CDI[4, 21], indicating that *Fusobacterium* may be prevalent during times of microbial dysbiosis. Finally, we also examined stool from pediatric IBD patients, all of whom harbored detectable *Fusobacterium* by qPCR. Stool supernatants from adult and pediatric CDI patients who tested positive for *Fusobacterium* were collected, diluted in aggregation buffer and aggregates were examined by FISH for *C. difficile* and *F. nucleatum* (Fig 3D). We observed co-localization of both species in the patient stool samples, indicating that *C. difficile* may interact with *Fusobacterium* in a subset of patients.

Based on our observation that *C. difficile* and *F. nucleatum* formed aggregates in patient stool samples, we reasoned that *C. difficile* may be chemoattracted to *F. nucleatum*. To

address this hypothesis, we examined chemotaxis of fluorescently-tagged *C. difficile* R20219 towards *F. nucleatum* subspecies (*nucleatum, polymorphum* and *animalis*) using a standard capillary chemotaxis assay (Fig. 4A). After 1 hr incubation, *C. difficile* was found to enter capillary tubes containing *F. nucleatum* subspecies. To elucidate how *F. nucleatum* influences *C. difficile*, we performed a global transcriptional analysis of *C. difficile* R20291 incubated with *F. nucleatum* metabolites (Fig. 4B-G). Overall, 286 *C. difficile* genes were upregulated in response to *F. nucleatum* and 20 genes were downregulated (Fig. 4B). Among upregulated gene clusters in *C. difficile*, genes encoding chemotaxis, antimicrobial resistance, cell wall components, and metabolism, were observed (Fig. 4C-F). Consistent with our chemotaxis data, we found that 7 upregulated genes were related to bacterial chemotaxis (*fliE, flbD, flgG, fliK, fliN, fliS*)(Fig. 4C). We also found increased expression of 13 of 19 ethanolamine utilization genes in *C. difficile* in response to *F. nucleatum* metabolites (Fig. 4G). Ethanolamine has been previously reported to modulate *C. difficile* pathogenesis[25] and is a chemotactic agent for other enteric pathogens. In a chemotaxis assay, *C. difficile* strains R20291, 630 and 196 were found to be attracted to 15 mM ethanolamine (Fig. 4H). These findings suggest that chemical signals may mediate interactions between *C. difficile* and *F. nucleatum*.

Bacterial surface adhesion and co-aggregation is essential for the development of multispecies biofilm communities[18]. To assess co-aggregation between *C. difficile* and *F. nucleatum*, strains were incubated in aggregation buffer for 1 hour and cell:cell aggregation was monitored by optical density ($OD6_{00nm}$). Aggregation of co-incubated strains compared to independently incubated controls was calculated based on the OD_{600} at time 0 and after 1 hr of anaerobic incubation at 37°C. *C. difficile* R20291 alone had minimal auto-aggregation (9.5 ± 1.2) compared to *F. nucleatum* subspecies *nucleatum* auto-aggregation (37.4 ± 4). However, co-incubation resulted in 61.8 ± 1% aggregated cells (Fig. 5A). *F. nucleatum* is known to express several proteins involved in adhesion, including lectin Fap2 which binds to Gal-GalNac[26], and RadD which has been characterized as an arginine-dependent adhesin[27]. To elucidate the role of surface adhesion proteins in co-aggregation, *F. nucleatum* subspecies *nucleatum* was pre-incubated with either neutral glucose, Fap2-inhibiting galactose or RadD-inhibiting arginine[27]. While no impact on aggregation was observed in the presence of glucose or galactose (Fig. 5A), pre-incubation with arginine blocked co-aggregation, suggesting that RadD is a mediator of *C. difficile-F. nucleatum* adhesion. In a parallel approach, aggregation of *C. difficile* with *F. nucleatum* strains lacking either RadD or Fap2, were compared to aggregation of wild-type *F. nucleatum* (Fig. 5B). In agreement with our observation that pre-incubation with galactose did not effectively block co-aggregation, *C. difficile* strains incubated with *F. nucleatum* strains lacking Fap2 only exhibited a modest reduction in aggregation, while strains lacking RadD yielded reduced aggregation (Fig. 5B). This aggregation can be appreciated visually in cuvettes (Fig. 5C), where *C. difficile* alone remains un-aggregated and addition of wild-type *F. nucleatum* to *C. difficile* causes an accumulation of aggregates at the bottom of the cuvette. Similar to our aggregation calculations, the Fap2 mutant aggregates with *C. difficile*, while the RadD mutant has reduced aggregation with *C. difficile*. Microscopy of fluorescently-tagged bacteria also demonstrated the ability of wild-type *F. nucleatum* subspecies *nucleatum* to form aggregates with *C. difficile*, while *F. nucleatum* subspecies *nucleatum ΔradD* failed to exhibit the same

degree of aggregation with *C. difficile* (Fig. 5D). Taken together, these data indicate that RadD is the primary mediator of *C. difficile-F. nucleatum* inter-microbial adhesion.

To investigate the conservation of co-aggregation of *C. difficile* to a broad range of *F. nucleatum* subspecies, aggregation assays were performed using *F. nucleatum* subspecies *polymorphum* and *animalis* (Fig. 5E,F). Consistent with our *F. nucleatum* subspecies *nucleatum* data, *C. difficile* strains also co-aggregated with *F. nucleatum* subspecies *polymorphum* and *animalis* (Fig. 5E,F). Of note, *C. difficile* exhibited the lowest aggregation with *F. nucleatum* subspecies *animalis*, which is the least auto-aggregative of the three species. Next, we examined the aggregation of *C. difficile* with other gut microbes to determine if aggregation was a unique feature of *C. difficile* and *F. nucleatum*. We analyzed 10 different intestinal microbes representing the phyla Firmicutes, Bacteroidetes, Actinobacteria, Proteobacteria and Verrucomicrobia (Supplemental Fig. 2A). No microbes were identified that had enhanced aggregation with *C. difficile*. Since flagella are important for host adhesion, we asked whether flagella could mediate the interaction between *C. difficile* and *F. nucleatum* RadD. To address this question, we sheared the flagella from *C. difficile* R20291 and examined aggregation of sheared flagella or flagella-free *C. difficile* with *F. nucleatum* subspecies *nucleatum* (Supplemental Fig. 2B). *F. nucleatum* was observed to aggregate to a similar degree with sheared flagella and intact *C. difficile*. Moreover, flagella-free *C. difficile* exhibited decreased aggregation with *F. nucleatum* compared to intact *C. difficile*. These data indicate that *C. difficile* flagella adhere to *F. nucleatum* RadD.

To determine if *C. difficile* and *F. nucleatum* would preferentially aggregate in the presence of the intestinal epithelium, fluorescently-tagged bacteria were incubated with mucin-producing HT29-MTX cells for 1 hour and then examined by microscopy (Fig. 6A). *F. nucleatum* subspecies *nucleatum, polymorphum* and *animalis*, as well as *F. nucleatum* subspecies *nucleatum Δfap2* co-localized with *C. difficile* R20291 above the epithelium. In contrast, minimal aggregation was observed with *C. difficile* and *F. nucleatum* subspecies *nucleatum ΔradD* on HT29-MTX cells. We also confirmed this aggregation profile using human colonoids, where a similar pattern was observed (Fig. 6B). Finally, FISH analysis of surgical resections from patients with recurrent CDI revealed co-localization of *C. difficile* and *Fusobacterium* in the mucus layer above the epithelium (Fig. 6C). These data establish that *C. difficile* interacts with the *F. nucleatum* surface adhesin RadD to promote aggregation and that these two species aggregate in the mucus layer.

Aggregation is the initiating process in biofilm development, which is an important factor in colonization. Since we observed significant aggregation between *C. difficile* and *F. nucleatum*, we next sought to determine if *F. nucleatum* influenced *C. difficile* biofilm formation. Biofilm density present on MUC2-coated coverslips was visualized by ruby red biofilm tracer (Fig. 7A). Consistent with our aggregation data, wild-type *F. nucleatum* subspecies *nucleatum* enhanced *C. difficile* biofilm formation. The *F. nucleatum* subspecies *nucleatum ΔradD* derivative failed to enhance biofilm formation to the same degree as the wild-type strain (Fig 7A, Supplemental Fig. 3A). Examination of biofilms by scanning electron microscopy revealed the additive effect of *F. nucleatum* subspecies *nucleatum* on biofilm formation (Fig. 7B-D). Importantly, biofilms contain both *C. difficile* and *F. nucleatum*, as seen in the pseudo-colored SEM (Fig. 7D), indicating that *F. nucleatum* and

C. difficile likely have a synergistic relationship. *F. nucleatum* subspecies *polymorphum* and *animalis* also enhanced biofilm for all *C. difficile* strains (Supplemental Fig. 3B,C), further supporting our hypothesis that these interactions are broadly conserved. To assess which components of the biofilm were enhanced by *F. nucleatum*, we examined the major components of biofilm: DNA, proteins and polysaccharides (Supplemental Fig. 4A-C). Co-cultures with *C. difficile* and *F. nucleatum* exhibited increased DNA, proteins and soluble extracellular polysaccharides (EPS) compared to either *C. difficile* alone or *C. difficile-F. nucleatum* subspecies *ΔradD* biofilms. No changes were observed in insoluble extracellular polysaccharides (IEPS) or intracellular polysaccharides (IPS) (Supplemental Fig. 4C). Finally, we sought to determine if *F. nucleatum* enhancement of *C. difficile* biofilms had an effect on biofilm stability. Biofilms harboring both *C. difficile* and *F. nucleatum* were more resistant to Proteinase K, DNAse, EDTA and the antibiotic vancomycin (Supplemental Fig. 4D). Collectively, this work points to *F. nucleatum* as an interacting member of the mucus-associated microbiome that promotes *C. difficile* aggregation and enhances biofilm formation.

Discussion:

Recent in-depth analysis of the gut microbiome has revealed that intestinal disorders are often polymicrobial in origin or manifestation[28]. Polymicrobial interactions are particularly important in the setting of infection and chronic disease, as microbes can interact synergistically to induce virulence traits, modify the environmental niche, or modulate the host immune response. In the setting of *C. difficile* infection, these interactions are incompletely understood. Here we show that *F. nucleatum* adheres to *C. difficile*, influences key genes in *C. difficile* for chemotaxis and niche development, and promotes aggregation and biofilm formation. These findings were replicated using eleven *C. difficile* strains and three *F. nucleatum* subspecies, indicating the shared abilities of these strains to interact with each other. This work also identified RadD and flagella as key adhesins involved in bacterial-bacterial interactions between *C. difficile* and *F. nucleatum*.

F. nucleatum is well-characterized in the oral cavity, where it forms highly structured, multispecies communities that can promote oral diseases like gingivitis/periodontitis[18]. *F. nucleatum* adheres to several oral Gram-positive microbes, so it is unlikely that the interaction between *F. nucleatum* and *C. difficile* is unique. However, one interesting feature of *F. nucleatum* and *C. difficile* is horizontal gene transfer. Genome analysis of *F. nucleatum* subspecies *polymorphum* ATCC 10953 found that 16 conserved gene clusters were from *C. difficile*[29]. Additionally, it appears that *F. nucleatum* subspecies *polymorphum* has obtained 5 composite ribozyme/transposons, similar to *C. difficile's* CdISt-IStrons. These data support our hypothesis that these two species can act synergistically.

Although oral bacteria poorly colonize the healthy intestine, increased quantities of oral microbes, including *Fusobacterium*, have been reported in the gut microbiota of patients following antibiotic intake[30-33]. Consistent with these studies, our analysis of published 16S rRNA gene data sets[4, 21] indicate that healthy subjects typically harbor lower *Fusobacterium* abundances. *Fusobacterium* has also been isolated from the intestinal mucus-associated microbiota of IBD patients, a population that experiences increased morbidity in terms of *C.*

difficile infection[34]. Data from our pediatric cohort supports potential interactions between *C. difficile* and *F. nucleatum* in IBD patients. Although we do not have data on outcomes of patients harboring greater numbers of *Fusobacterium* OTUs, we speculate that *F. nucleatum* may be a confounding or disease-modifying factor in *C. difficile* infection since this species promotes robust biofilm formation.

Our RNAseq data revealed that *C. difficile* ethanolamine related genes in response to *F. nucleatum* metabolites. Ethanolamine is an end-product of phosphatidylethanolamine catabolism, an abundant phospholipid in both mammalian and bacterial membranes. Other GI pathogens, including enterohemorrhagic *Escherichia coli* (EHEC) and *Salmonella*, recognize ethanolamine as a signal to modulate virulence and colonization gene expression[35, 36]. Ethanolamine also impacts *C. difficile* pathogenesis[25, 37]. *F. nucleatum* encodes three glycerolphosphoryl diester phosphodiesterase proteins (FN1891, FN1908, and FN1954) that can generate ethanolamine[38]. While ethanolamine membrane diffusion in other microbial species is low, diffusion is amplified by *F. nucleatum's* ethanolamine permease (FN0089)[39]. Similar to our findings, *F. nucleatum* upregulates ethanolamine utilization genes in the oral microbe *S. gordonii*[38]. As a result, we speculate that intestinal *F. nucleatum*-produced ethanolamine can influence *C. difficile* and perhaps modulate pathogenesis.

Interactions between *C. difficile* and *F. nucleatum* are of key interest because of the potential impact each strain may have on the host and on each other. We speculate that interspecies interactions could be some of the earliest events that occur as *C. difficile* colonizes the host. As a result, we believe that an improved understanding of how *C. difficile* interacts with mucus-associated microbes will continue to clarify the mechanisms of CDI.

Supplementary Material

Refer to Web version on PubMed Central for supplementary material.

Acknowledgments

We would like to thank Dr. Xi-Lei Zeng for her expertise and preparation of the colonoid monolayers used in this study. We would also like to thank Dr. Chenggang Wu at UT Health for his intellectual input on the project.

Funding: This work was supported by grants from the National Institute of Diabetes and Digestive and Kidney Diseases (Grant P30-DK-56338 to Texas Medical Center Digestive Disease Center, Gastrointestinal Experimental Model Systems), National Institutes of Health (NIH) K01DK12319501 (MAE), KO1DK12186901 (ACE), T32DK07644 (WR), F32AI136404 (HAD), R01AI123278 (RAB), U01AI124290 (RAB, KWG, TS), and unrestricted research support from BioGaia AB (RAB, JV, Stockholm, Sweden).

Data Availability Statement :

The raw data supporting the conclusions of this manuscript can be found under the following BioSample accession numbers: SAMN15790567, SAMN15790568, SAMN15790569, SAMN15790570, SAMN15790571, SAMN15790572.

References:

1. Dubberke ER, Carling P, Carrico R, et al. Strategies to prevent Clostridium difficile infections in acute care hospitals: 2014 update. Infect Control Hosp Epidemiol 2014;35 Suppl 2:S48–65.
2. Leffler DA, Lamont JT. Clostridium difficile Infection. N Engl J Med 2015;373:287–8.
3. Schneider D, Thurmer A, Gollnow K, et al. Gut bacterial communities of diarrheic patients with indications of Clostridioides difficile infection. Sci Data 2017;4:170152. [PubMed: 29039846]
4. Schubert AM, Rogers MA, Ring C, et al. Microbiome data distinguish patients with Clostridium difficile infection and non-C. difficile-associated diarrhea from healthy controls. MBio 2014;5:e01021–14. [PubMed: 24803517]
5. Semenyuk EG, Poroyko VA, Johnston PF, et al. Analysis of Bacterial Communities during Clostridium difficile Infection in the Mouse. Infect Immun 2015;83:4383–91. [PubMed: 26324536]
6. Engevik MA, Yacyshyn MB, Engevik KA, et al. Human Clostridium difficile infection: altered mucus production and composition. Am J Physiol Gastrointest Liver Physiol 2015;308:G510–24. [PubMed: 25552581]
7. Engevik MA, Luk B, Chang-Graham AL, et al. Bifidobacterium dentium Fortifies the Intestinal Mucus Layer via Autophagy and Calcium Signaling Pathways. mBio 2019;10.
8. Yamakawa K, Kamiya S, Meng XQ, et al. Toxin production by Clostridium difficile in a defined medium with limited amino acids. J Med Microbiol 1994;41:319–23. [PubMed: 7966203]
9. Bainer R, Park H, Cluzel P. A high-throughput capillary assay for bacterial chemotaxis. J Microbiol Methods 2003;55:315–9. [PubMed: 14500024]
10. Park J, Shokeen B, Haake SK, et al. Characterization of Fusobacterium nucleatum ATCC 23726 adhesins involved in strain-specific attachment to Porphyromonas gingivalis. International Journal of Oral Science 2016;8:138–144.
11. Landry RM, An D, Hupp JT, et al. Mucin-Pseudomonas aeruginosa interactions promote biofilm formation and antibiotic resistance. Mol Microbiol 2006;59:142–51. [PubMed: 16359324]
12. Chang-Graham AL, Danhof HA, Engevik MA, et al. Human Intestinal Enteroids With Inducible Neurogenin-3 Expression as a Novel Model of Gut Hormone Secretion. Cell Mol Gastroenterol Hepatol 2019;8:209–229. [PubMed: 31029854]
13. Aires CP, Del Bel Cury AA, Tenuta LM, et al. Effect of starch and sucrose on dental biofilm formation and on root dentine demineralization. Caries Res 2008;42:380–6. [PubMed: 18781066]
14. Robinson CD, Auchtung JM, Collins J, et al. Epidemic Clostridium difficile strains demonstrate increased competitive fitness compared to nonepidemic isolates. Infect Immun 2014;82:2815–25. [PubMed: 24733099]
15. Wattam AR, Davis JJ, Assaf R, et al. Improvements to PATRIC, the all-bacterial Bioinformatics Database and Analysis Resource Center. Nucleic Acids Res 2017;45:D535–D542. [PubMed: 27899627]
16. Karygianni L, Follo M, Hellwig E, et al. Microscope-based imaging platform for large-scale analysis of oral biofilms. Appl Environ Microbiol 2012;78:8703–11. [PubMed: 23042171]
17. Sato T, Stange DE, Ferrante M, et al. Long-term expansion of epithelial organoids from human colon, adenoma, adenocarcinoma, and Barrett's epithelium. Gastroenterology 2011;141:1762–72. [PubMed: 21889923]
18. He X, Hu W, Kaplan CW, et al. Adherence to streptococci facilitates Fusobacterium nucleatum integration into an oral microbial community. Microb Ecol 2012;63:532–42. [PubMed: 22202886]
19. Fukugaiti MH, Ignacio A, Fernandes MR, et al. High occurrence of Fusobacterium nucleatum and Clostridium difficile in the intestinal microbiota of colorectal carcinoma patients. Braz J Microbiol 2015;46:1135–40. [PubMed: 26691472]
20. Khanna S, Montassier E, Schmidt B, et al. Gut microbiome predictors of treatment response and recurrence in primary Clostridium difficile infection. Aliment Pharmacol Ther 2016;44:715–727. [PubMed: 27481036]
21. Battaglioli EJ, Hale VL, Chen J, et al. Clostridioides difficile uses amino acids associated with gut microbial dysbiosis in a subset of patients with diarrhea. Sci Transl Med 2018;10.

22. Seekatz AM, Rao K, Santhosh K, et al. Dynamics of the fecal microbiome in patients with recurrent and nonrecurrent Clostridium difficile infection. Genome Med 2016;8:47. [PubMed: 27121861]
23. Davido DJ, Richter F, Boxberger F, et al. Butyrate and propionate downregulate ERK phosphorylation in HT-29 colon carcinoma cells prior to differentiation. Eur J Cancer Prev 2001;10:313–21. [PubMed: 11535873]
24. Khanna R, Chande N, Nelson RL. Treatment of an initial infection with clostridium difficile in patients with inflammatory bowel disease. Inflamm Bowel Dis 2013;19:2223–6. [PubMed: 23929262]
25. Nawrocki KL, Wetzel D, Jones JB, et al. Ethanolamine is a valuable nutrient source that impacts Clostridium difficile pathogenesis. Environ Microbiol 2018;20:1419–1435. [PubMed: 29349925]
26. Abed J, Emgard JE, Zamir G, et al. Fap2 Mediates Fusobacterium nucleatum Colorectal Adenocarcinoma Enrichment by Binding to Tumor-Expressed Gal-GalNAc. Cell Host Microbe 2016;20:215–25. [PubMed: 27512904]
27. Kaplan CW, Lux R, Haake SK, et al. The Fusobacterium nucleatum outer membrane protein RadD is an arginine-inhibitable adhesin required for inter-species adherence and the structured architecture of multispecies biofilm. Mol Microbiol 2009;71:35–47. [PubMed: 19007407]
28. Tay WH, Chong KK, Kline KA. Polymicrobial-Host Interactions during Infection. J Mol Biol 2016;428:3355–71. [PubMed: 27170548]
29. Karpathy SE, Qin X, Gioia J, et al. Genome sequence of Fusobacterium nucleatum subspecies polymorphum - a genetically tractable fusobacterium. PLoS One 2007;2:e659. [PubMed: 17668047]
30. Brennan CA, Garrett WS. Fusobacterium nucleatum - symbiont, opportunist and oncobacterium. Nat Rev Microbiol 2019;17:156–166. [PubMed: 30546113]
31. Strauss J, Kaplan GG, Beck PL, et al. Invasive potential of gut mucosa-derived Fusobacterium nucleatum positively correlates with IBD status of the host. Inflamm Bowel Dis 2011;17:1971–8. [PubMed: 21830275]
32. Lee Y, Eun CS, Lee AR, et al. Fusobacterium Isolates Recovered From Colonic Biopsies of Inflammatory Bowel Disease Patients in Korea. Ann Lab Med 2016;36:387–9. [PubMed: 27139617]
33. de Meij TGJ, de Groot EFJ, Peeters CFW, et al. Variability of core microbiota in newly diagnosed treatment-naive paediatric inflammatory bowel disease patients. PLoS One 2018;13:e0197649. [PubMed: 30102706]
34. Balram B, Battat R, Al-Khoury A, et al. Risk Factors Associated with Clostridium difficile Infection in Inflammatory Bowel Disease: A Systematic Review and Meta-Analysis. J Crohns Colitis 2019;13:27–38. [PubMed: 30247650]
35. Gonyar LA, Kendall MM. Ethanolamine and choline promote expression of putative and characterized fimbriae in enterohemorrhagic Escherichia coli O157:H7. Infect Immun 2014;82:193–201. [PubMed: 24126525]
36. Kendall MM, Gruber CC, Parker CT, et al. Ethanolamine controls expression of genes encoding components involved in interkingdom signaling and virulence in enterohemorrhagic Escherichia coli O157:H7. MBio 2012;3.
37. Janoir C, Deneve C, Bouttier S, et al. Adaptive strategies and pathogenesis of Clostridium difficile from in vivo transcriptomics. Infect Immun 2013;81:3757–69. [PubMed: 23897605]
38. Hendrickson EL, Wang T, Beck DA, et al. Proteomics of Fusobacterium nucleatum within a model developing oral microbial community. Microbiologyopen 2014;3:729–51. [PubMed: 25155235]
39. Garsin DA. Ethanolamine utilization in bacterial pathogens: roles and regulation. Nat Rev Microbiol 2010;8:290–5. [PubMed: 20234377]

WHAT YOU NEED TO KNOW:

Background: *Clostridium difficile* is an enteric pathogen that causes diarrhea and life-threatening inflammation. *C. difficile* infection is accompanied by changes in the gut microbiota; however, it is unclear how these microbes influence *C. difficile*.

New Findings: Using bioreactors, patient stool, and human colonoids, we demonstrate that *C. difficile* aggregates with the opportunist pathogen *Fusobacterium nucleatum*. Moreover, these species form robust biofilms that depend on the *Fusobacterium* protein RadD.

Limitations: We do not have data on outcomes of patients harboring greater numbers of *Fusobacterium* OTUs, although we speculate that *F. nucleatum* may be a confounding factor in *C. difficile* infection.

Impact: This work indicates that *F. nucleatum* acts synergistically with *C. difficile* in the mucus layer. As a result, *F. nucleatum* should be considered when addressing *C. difficile* infection, especially in populations known to harbor higher *Fusobacterium* levels.

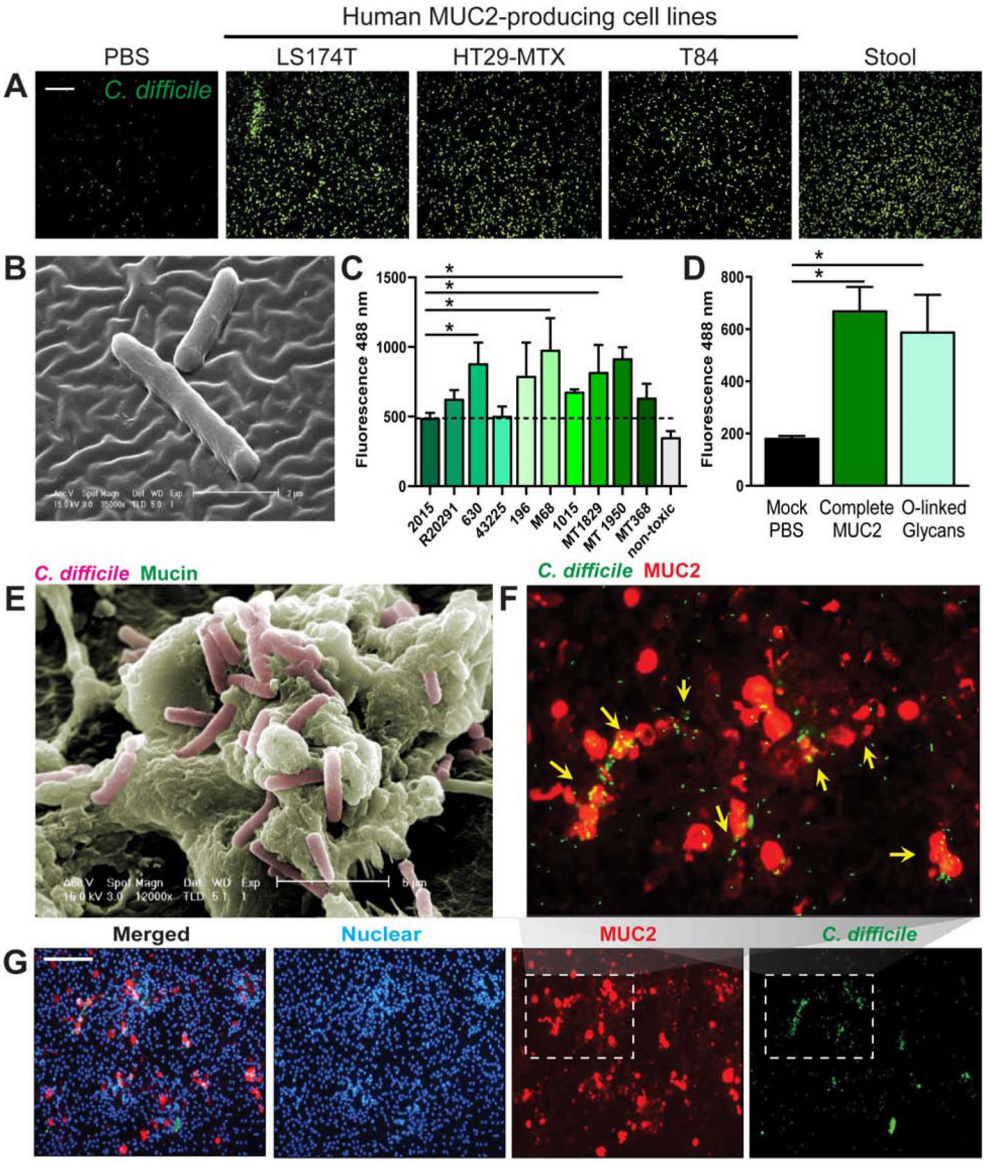

Figure 1: *C. difficile* adheres to purified human MUC2.

MUC2 was isolated from the supernatants of mucin-producing cell lines LS174T, HT29-MTX and T84, as well as from stool from healthy volunteers by a series of CsCl ultracentrifugation steps. MUC2 (1 mg/mL) was applied to coverslips linked via APTS. *C. difficile* R20291 was fluorescently-tagged with CFDA-SE and incubated with mucus-coated coverslips for 1 hour. **A**. Adhesion was visualized by microscopy (scale bar =50 μm) (representative image from n=4 replicates/repeated 3 independent times). **B**. Scanning electron microscopy of APTS-MUC2 coated coverslips demonstrating adhesion of *C. difficile* to HT29-MTX-derived MUC2 (representative image; n=3). **C**. Fluorescently-tagged *C. difficile* was added to 96-well plates coated with MUC2 purified from HT29-MTX and fluorescence values were obtained using a plate reader (n=8 replicates/repeated 3 independent times). **D.** Adhesion of *C. difficile* R20291 to mock (PBS), purified intact MUC2 or isolated MUC2-derived O-linked glycans (n=4 replicates/repeated 2 independent

times). **E.** Co-localization of *C. difficile* and MUC2 in LS174T cells was also demonstrated by scanning electron microcopy (SEM) (representative image; n=3). **F,G.** CFDA-SE labeled *C. difficile* (green) was also found to co-localize with MUC2 (red) positive goblet cells in human colonoid monolayers by immunostaining (scale bar= 100 μM), which is clearly observed in the expanded inset above (**F**) (n=3 replicates, repeated 2 independent times). ANOVA, *p<0.05.

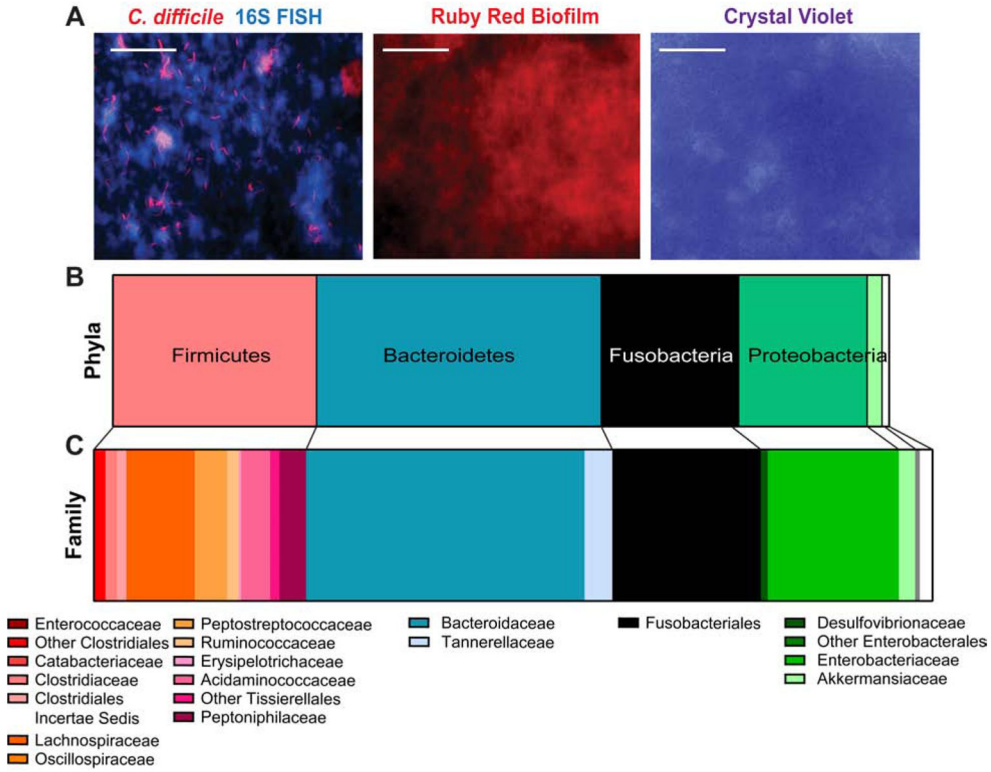

Figure 2: *C. difficile* interacts with other mucus-associated microbes in bioreactor mucin-based biofilms.

Bioreactors were modified with a hanging insert containing MUC2-APTS-coated cover slips. Bioreactors were seeded with stool from healthy volunteers (2x donors, 3x fecal pools, n =4) and treated with clindamycin (250 μg/mL) followed by *C. difficile* (10^6 CFU). MUC2 coated inserts were examined for biofilm production, *C. difficile* localization and 16S rRNA sequencing. **A.** FISH immunostaining for *C. difficile* (red) and total 16S rRNA genes (all bacteria; blue). Biofilms on coverslips were stained with ruby red biofilm tracer and crystal violet staining (scale bar = 50 μm) (representative image; n=4/stain). The composition of mucin-coated inserts was examined by 16S sequencing which revealed a unique microbial community at the phylum (**B**) and family (**C**) level.

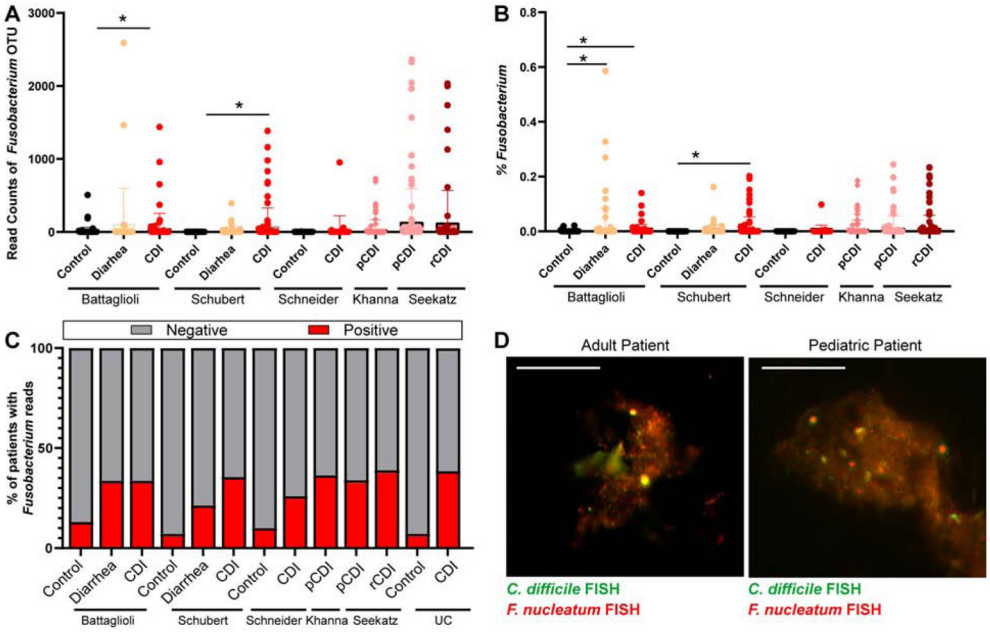

Figure 3: *Fusobacterium* is present in a subset of patients with *C. difficile* infection (CDI).

16S rRNA genes in stool from published databases[3, 4, 20-22] were examined for (**A**) number and (**B**) % abundance of *Fusobacterium* OTU reads. Samples included undefined CDI, recurrent CDI (rCDI) or primary CDI (pCDI) and age-matched controls (Battaglioli: control n=109, diarrhea n=114, CDI n=84; Schubert: control n=154, diarrhea n=89, CDI n=92; Schneider: control n=50, CDI n=29; Khanna pCDI n=88; Seekatz pCDI=148, rCDI n=82). **C**. Percentage analysis of patients who harbor *Fusobacterium* OTUs (positive, red) and patients without *Fusobacterium* OTUs (negative, grey) from previously published databases and a University of Cincinnati patient cohort (UC: control n=23, CDI n=59). Approximately 33.2% (averaged from all studies) of CDI patients had *Fusobacterium* reads. **D.** Aggregation of *C. difficile* and *Fusobacterium* in stool from adult patients with CDI (n=8) or pediatric patients with CDI and inflammatory bowel disease (IBD) (n=4) was examined by FISH using a probe for *C. difficile* (green) and *Fusobacterium* (red) (scale bar =50 μm). A representative image from an adult and pediatric patient are shown.

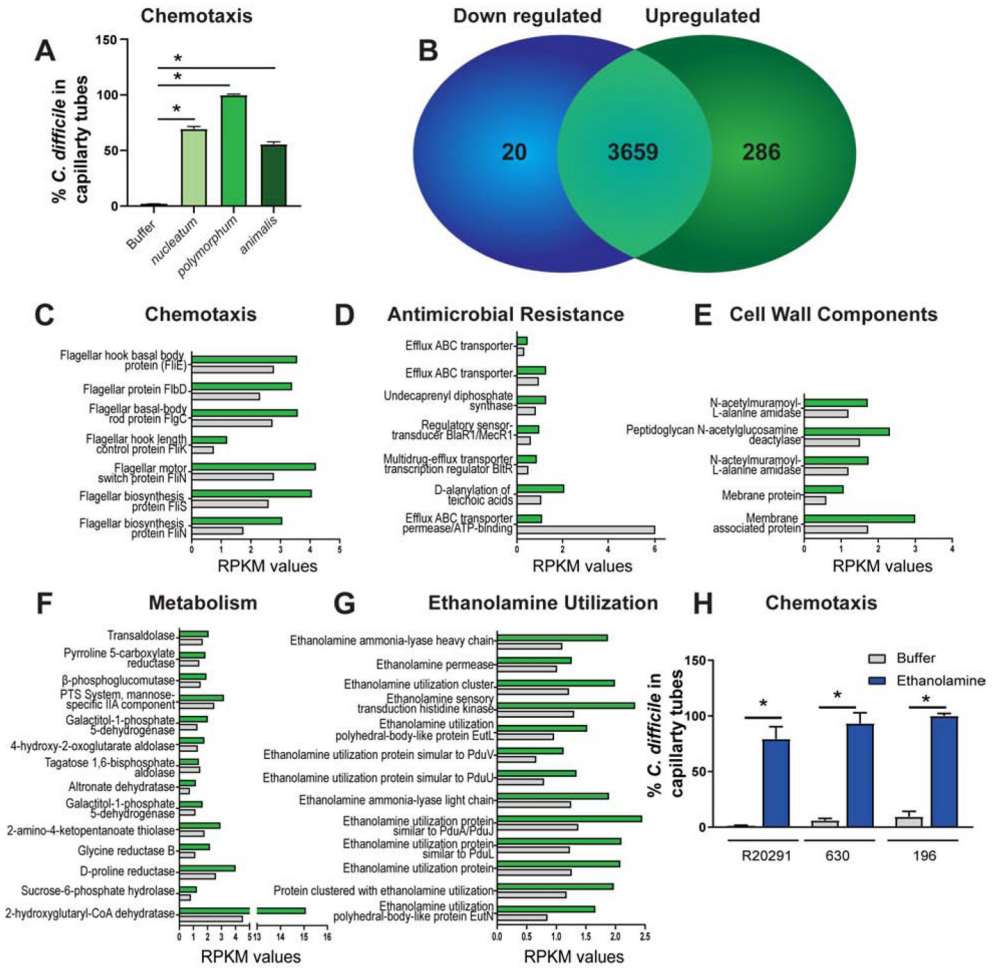

Figure 4: *F. nucleatum* metabolites influence *C. difficile* chemotaxis and gene expression.

A. Chemotaxis of fluorescently-tagged *C. difficile* R20291 into capillary tubes containing *F. nucleatum* subspecies *nucleatum, polymorphum* and *animalis* over 1 hr incubation (n=5 replicates, repeated 4 independent times). **B-G**. RNAseq analysis of pooled samples (n=3) of *C. difficile* after incubation with *F. nucleatum* subspecies *polymorphum* spent media (green bars) or *C. difficile* spent media (grey bars). **B**. 20 genes were downregulated and 286 genes were upregulated. *C. difficile* genes upregulated in response to *F. nucleatum* metabolites included (**C**) chemotaxis, (**D**) antimicrobial resistance, (**E**) cell wall components, (**F**) metabolism and (**G**) ethanolamine utilization. Data expressed as Reads Per Kilobase of transcript, per Million mapped reads (RPKM). **H**. Chemotaxis of fluorescently-tagged *C. difficile* strain R20291, 630 and 192 into capillary tubes containing 15 mM ethanolamine (n=5 replicates, repeated 3 independent times). One Way ANOVA, * $p < 0.05$.

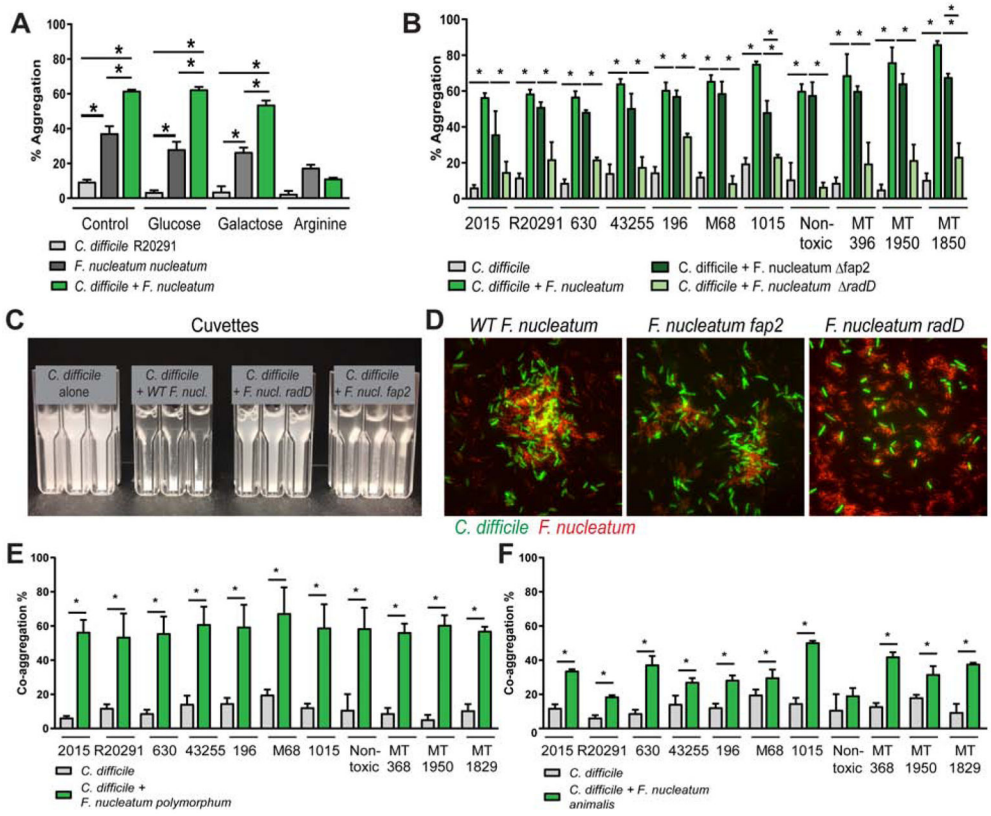

Figure 5: *F. nucleatum* aggregates with *C. difficile* via the adhesin RadD.

A. *C. difficile* R20291 and *F. nucleatum* subspecies *nucleatum* were incubated together anaerobically in co-aggregation buffer. Aggregation was calculated using the equation: 100%- ((OD_{600nm} at 0 hr –OD_{600nn} at 1 hr) x 100%). For inhibition assays, *F. nucleatum* subspecies *nucleatum* was pre-incubated for 5 min with 50 mM L-arginine, D-galactose, or D-glucose anaerobically, followed by addition of *C. difficile* (n=3-4 replicates, repeated 4 independent times). Significance was determined by Multi-way ANOVA. **B**. Aggregation was examined with 11 *C. difficile* strains, wild-type *F. nucleatum* subspecies *nucleatum*, as well as *F. nucleatum* subspecies *nucleatum* Δ*fap2* and *F. nucleatum* subspecies *nucleatum* Δ*radD*. **C**. For visualization, cuvettes were examined for aggregation in *C. difficile* alone, *C. difficile* with wild-type *F. nucleatum* subspecies *nucleatum*, Δ*fap2* and Δ*radD*. **D.** Microscopy of CFDA-SE tagged *C. difficile* R20291 (green) and *F. nucleatum* subspecies *nucleatum* (wild-type (WT), *Δfap2* or *ΔradD*) (red) (scale bar =50 μm) (n=3). Co-aggregation was also examined with *C. difficile* strains and (**E**) *F. nucleatum* subspecies *polymorphum* and (**F**) *F. nucleatum* subspecies *animalis* (n=4 replicates, repeated 3 independent times). One Way ANOVA, * $p < 0.05$.

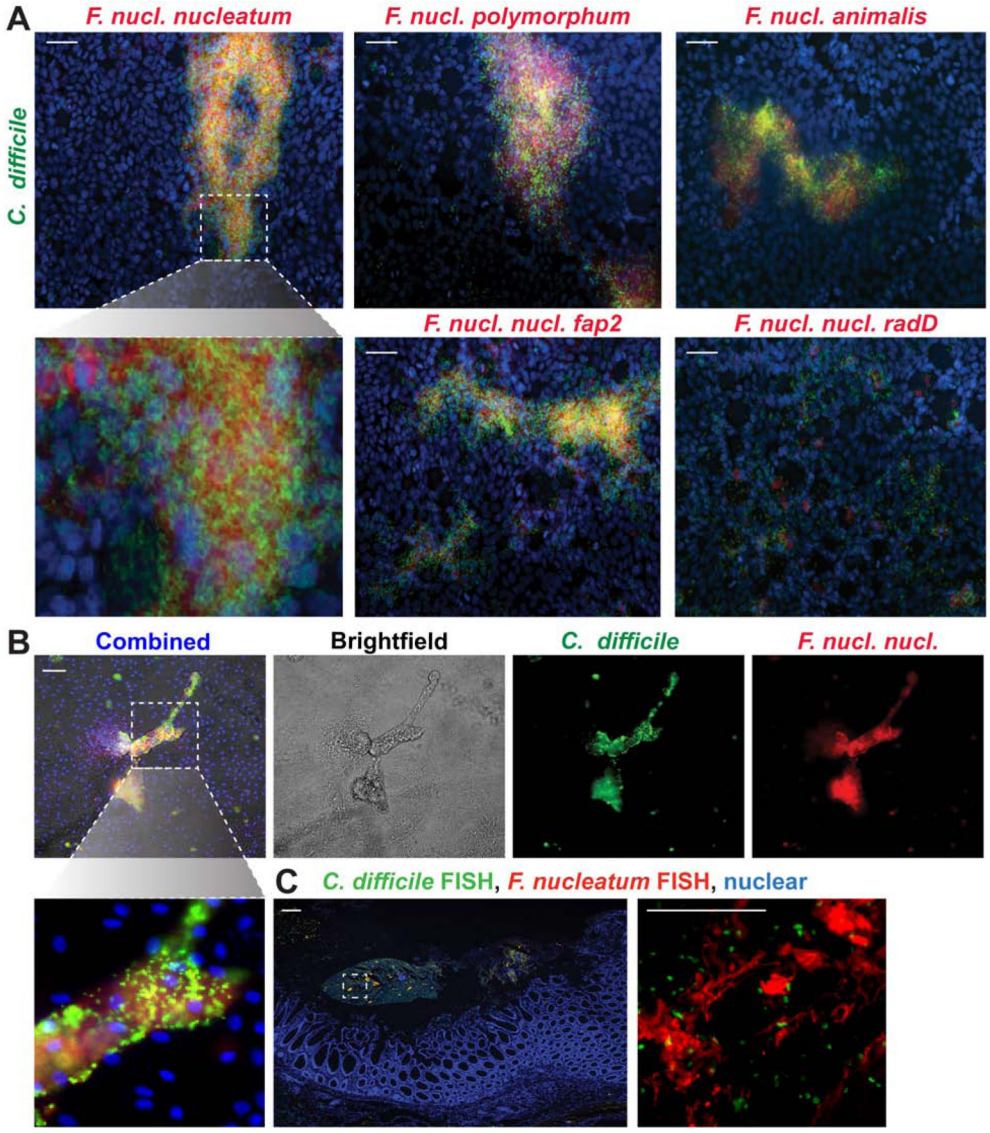

Figure 6. *F. nucleatum* strains aggregate with *C. difficile* R20291 on HT29-MTX cells and human colonoids.

A. Representative images of mucin producing HT29-MTX monolayers incubated with CFDA-SE fluorescently tagged *C. difficile* R20291 (green) and CMRA fluorescently-tagged *F. nucleatum* subspecies *nucleatum, nucleatum Δfap2*, *nucleatum ΔradD*, *polymorphum* or *animalis* (red) after 1 hr (scale bar =50 μm)(n=3 replicates, repeated 3 independent times). **B**. Representative images of human colonoids (organoids) incubated with *C. difficile* R20291 (green) and *F. nucleatum* subspecies *nucleatum* after 1 hr (scale bar =50 μm) (n=3 replicates, repeated 2 independent times). Higher magnification inset below highlights co-localization. **C**. Representative image of *C. difficile* and *Fusobacterium* FISH staining in surgical resections from patients with recurrent CDI (n=4 patients). Positive staining for *C. difficile* (green) and *Fusobacterium* (red) were observed at 40x (left) (scale bar = 50 μm) and 400x (inset right) (scale bar = 100 μm)

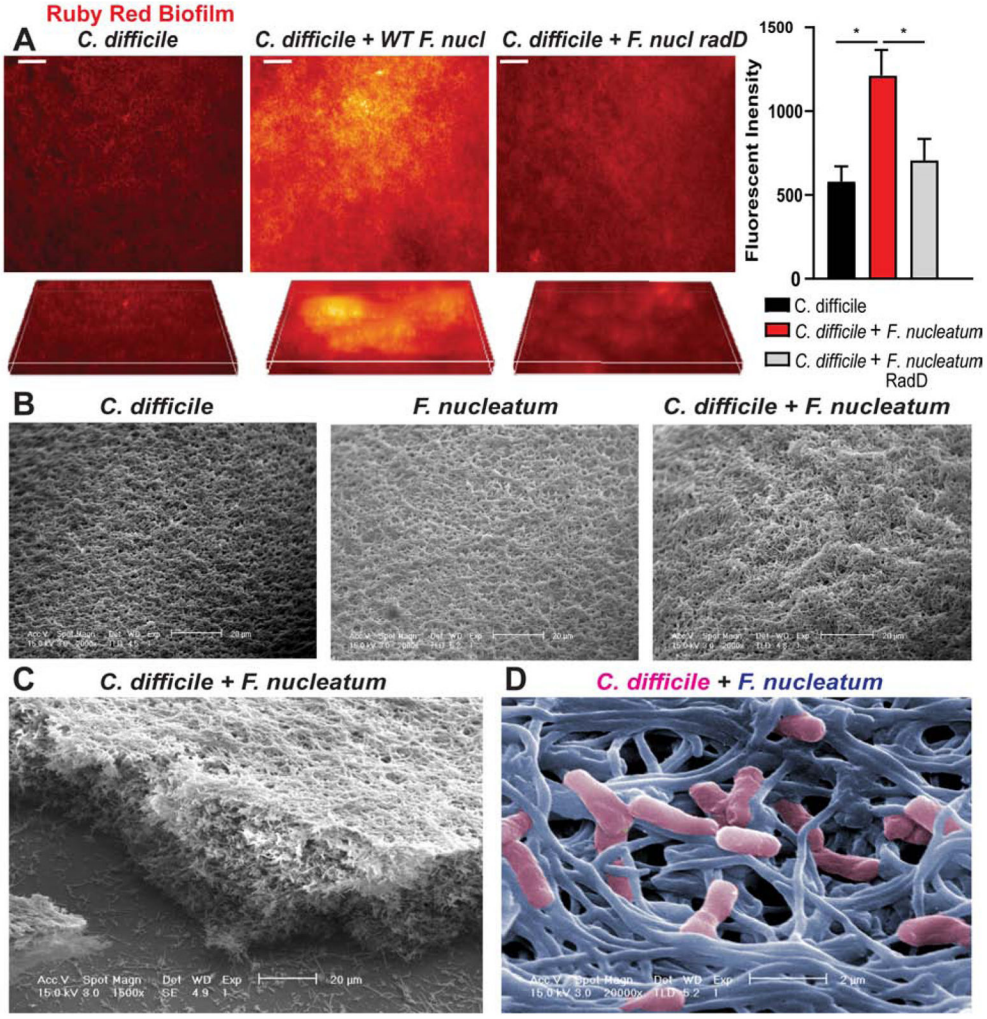

Figure 7. *F. nucleatum* bolsters *C. difficile* biofilms.

A. Biofilms of *C. difficile* R20291 with or without wild-type *F. nucleatum* subspecies *nucleatum* or *F. nucleatum* subspecies *nucleatum* Δ radD were grown on HT29-MTX-derived MUC2 coverslips anaerobically for 72 hrs. Biofilm extracellular matrix was visualized with ruby red biofilm tracer and examined with 2D and z-stack analysis (scale bar =50 μm)(n=3 replicates, repeated 3 independent times). Quantification performed by FIJI for relative fluorescent intensities. **B**. Scanning electron microscopy (SEM) of mucin-based biofilms (scale bar =20 μm) (representative image; n=3 replicates). **C.** Robust biofilms were observed via SEM by lateral views of *C. difficile* and *F. nucleatum* (scale bar =20 μm) (left image). **D**. Representative falsely colored SEM image with *C. difficile* (pink) and *F. nucleatum* (blue) (scale bar = 2 μm).